ADVANCED FUNCTIONAL MATERIALS



DOI: 10.1002/adfm.200800764

# Tuning the Unidirectional Electron Transfer at Interfaces with Multilayered Redox-active Supramolecular Bionanoassemblies**

By *Omar Azzaroni,* Marta Álvarez, Ahmed I. Abou-Kandil, Basit Yameen,* and *Wolfgang Knoll*

In this work, we present a new strategy to construct redox-active molecular platforms to be used as molecular rectifiers with tunable and amplifiable electronic readout. The approach is based on using ligand-receptor biological interactions to bioconjugate electroactive bio-inorganic building blocks onto metal electrodes. The stability of the self-assembled interfacial architecture is provided by multivalent macromolecular ligands that act as scaffolds for building-up the multilayered structures. The ability of these electroactive supramolecular architectures to generate a unidirectional current flow and tune the corresponding electronic readout was demonstrated by mediating and rectifying the electron transfer between redox donors in solution and the Au electrode. The redox centers incorporated into the assembled architecture in a topologically controlled manner are responsible for tuning the amplification of the rectified electronic readout, thus behaving as a tunable bio-supramolecular diode. Our experimental results obtained with these redox-active bio-supramolecular architectures illustrate the versatility of molecular recognition-directed assembly in combination with hybrid bio-inorganic building blocks to construct highly functional interfacial architectures.

## 1. Introduction

Designing strategies to tune and manipulate the electron transfer at interfaces has become a most relevant topic in nanotechnology for the construction of functional molecular assemblies.[1–3] This is in close connection to the development of molecular electronics where molecular-level systems duplicate functions of bulk electronic devices.[4–6]

In most cases the design of molecular electronics devices demands two essential requirements: i) the organization of chemical assemblies of signal-switchable functional units and ii) their integration with appropriate supports that allow for the electronic transduction of the activated chemical functionality.[7] As a consequence, creating new alternatives to construct molecule-based functional devices based on integrating functional building blocks into well-defined assemblies describing well-ordered supramolecular architectures is of mandatory importance.[8,9]

On the other hand, control over the directionality of electron transfer is a key feature in the design of interfacial architectures to be used as platforms in molecular electronics.[10] This control enables the generation of functions like the current rectifier that involves the unidirectional current flow across an interface.[11] At the molecular level, this has been accomplished by introducing diverse chemical functionalities into monolayer assemblies like Langmuir–Blodgett films[12] or self-assembled monolayers (SAM).[13] These results demonstrated that the molecular-level control of the chemical topology and the dimensions of the interfacial architectures is the key to enabling highly functional molecular devices that can be tailored for specific uses. This constitutes a remaining challenge in materials science related to the design and creation of specific supramolecular nanostructures displaying tailor-made shape and function.[14–15] Organizing assemblies on solid surfaces has been demonstrated to be a powerful strategy to generate functional interfaces with well-defined architecture, topology, and chemical functionality.[16] In different cases these ordered functional thin films were constructed using building blocks such as polymers, nanoparticles, and enzymes, thus facilitating the fabrication of organized assemblies with nanometer precision.[17–19]

A further challenge in molecular electronics constitutes the creation of interfacial architectures driven by molecular recognition between different functional building blocks. Molecular recognition and self-assembly dictate the rules by

[*] Dr. O. Azzaroni, Dr. M. Álvarez, Dr. A. I. Abou-Kandil, B. Yameen, Prof. Dr. W. Knoll
Max-Planck-Institut für Polymerforschung
Ackermannweg 10, Mainz 55128 (Germany)
E-mail: azzaroni@mpip-mainz.mpg.de
Dr. O. Azzaroni
Instituto de Investigaciones Fisicoquímicas Teóricas y Aplicadas (INIFTA)
CONICET, Universidad Nacional de La Plata
CC 16 – Suc 4, La Plata 1900, (Argentina)
E-mail: azzaroni@inifta.unlp.edu.ar

[**] O. A. acknowledges financial support from the Alexander von Humboldt Stiftung, the Max Planck Society and Centro Interdisciplinario de Nanociencia y Nanotecnología (CINN) (IP-PAE, ANPCyT, Argentina). M. Á. thanks Junta de Comunidades de Castilla la Mancha for a postdoctoral fellowship. B. Y. gratefully acknowledges financial support from Higher Education Commission (HEC) of Pakistan and Deutscher Akademischer Austauschdienst DAAD (Code #A/04/30795).

which different building blocks recognize each other and associate to assemble into ordered functional nanostructures. The formation of architectures by spontaneous assembly is the cornerstone of nanotechnology where the convergence of chemistry, physics, and biology plays a fundamental role. The generation of complex supramolecular architectures by a ''bottom-up'' process has been explored by different groups.[20–25] However, little is known about the generation of molecular electronic devices driven by the recognition-mediated spontaneous assembly of ''multivalent'' building blocks.[26,27] Multivalency is an important type of interaction in biological systems and is based on the interaction through multiple simultaneous molecular contacts.[28–30] The valency of a biological entity refers to the number of separate connections of the same kind that it can form with other entities through ligand/receptor interactions. Multivalency has been demonstrated a powerful and versatile self-assembly pathway with the ability to confer thermodynamic and kinetic stability to the assembled supramolecular complexes. A good example is represented by microorganisms exploiting multivalent interactions to remain strongly attached to host cells when exposed to shear forces from flowing liquids.[31]

In this work, we discuss the possibility of creating interfacial architectures capable of tailoring and tuning the unidirectional electron transfer across interfaces using different functional building blocks. Our approach is based on using hybrid bio-inorganic building blocks constituted by redox-labeled proteins. The inorganic part of the building block is responsible for the redox-active functionality and the biomolecule provides the molecular recognition properties. The building blocks are assembled into multilayered structures through the use of multivalent macromolecular scaffolds, which act a molecular Velcro capable of conferring stability to the functional multilayer assembly through strong ligand/receptor interactions.

## 2. Results and Discussion

### 2.1. Recognition-mediated Self-assembly of the Redox-active Interfacial Architecture

The preparation of molecular assemblies through biological interactions has been previously described by a number of research groups.[32–37] In our case, the platform to build-up the supramolecular assemblies was constructed by initially chemisorbing a binary mixed SAM on Au surfaces in order to create a biotinylated surface (Fig. 1, step 1). The platform was composed of biotin-terminated thiol (12-mercaptododecanoic-(8-biotinoylamido-3,6-dioxaoctyl)amide) and 11-mercapto-1-undecanol in a 1:9 ratio, thus giving the optimum coverage of biotin centers to achieve maximum binding of streptavidin (SAv).[38,39] This particular binary SAM leads to a OH– and biotin-terminated surface in which the protein can recognize the surface-confined biotin moiety. It is worth mentioning that this platform constituted of biotin ligands surrounded by OH groups does not evidence non-specific adsorption of SAv, as demonstrated in control and blank experiments reported by different groups.[38–41] The multilayer assembly was created using two building blocks: ferrocene-labeled streptavidin (Fc-SAv) and biotin-labeled polyallylamine (b-PAH). We used a quartz crystal microbalance with dissipation monitoring (QCM-D) to follow the growth of the multilayer assembly driven by the molecular recognition between both building blocks. Figure 2 shows the layer-by-layer assembly of Fc-SAv and b-PAH as measured by QCM-D at the seventh overtone. The Fc-SAv and b-PAH layers were assembled from 1 μM and 1 mg $mL^{-1}$ solutions in 0.1 M PBS buffer, respectively. A rinsing step between the assemblies of the different layers was included in order to remove any unbound polyelectrolyte or protein remaining on the substrate. A stable baseline was first measured for the biotinylated gold-coated quartz crystal in contact with 0.1 M PBS buffer. Then, the Fc-SAv solution was injected into the QCM-D chamber. A rapid decrease in frequency was observed due to the conjugation of the redox-labeled protein onto the ligand-modified substrate. The Fc-SAv solution was in contact with the biotin-terminated surface for approximately 40 min. This enables the formation of a protein layer on the Au surface.

The frequency changes were accompanied with minute changes in dissipation indicating that the first Fc-SAv resembles a rather compact and rigid film. It is worth mentioning that sharp changes in frequency and dissipation should not simply be attributed to the significant increase in mass coverage of bioconjugated Fc-SAv. The rapid exchange

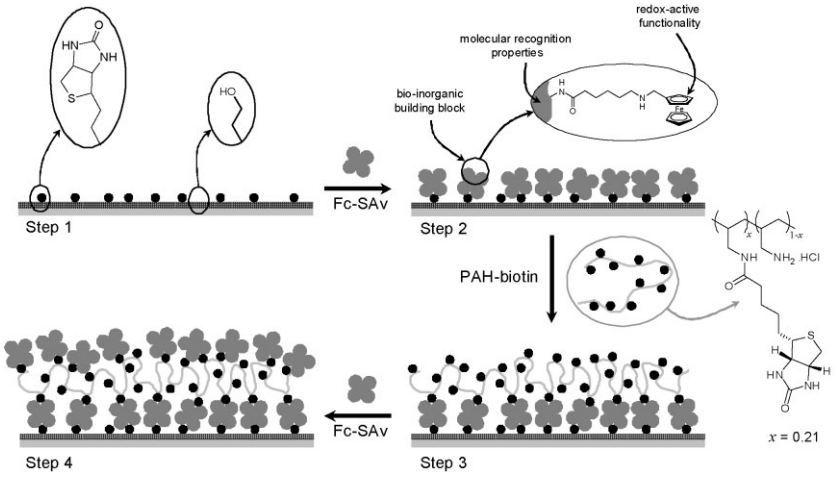


**Figure 1.** Simplified cartoon depicting the supramolecular assembly of the redox-active multilayers. The scheme describes the biotinylation of the Au electrode (step 1), the conjugation of the ferrocene-labeled streptavidin (Fc-SAv) (step 2), the conjugation of biotin-modified PAH (step 3), and the conjugation of the second layer of Fc-SAv (step 4). The chemical structures of the redox center and the multivalent macromolecular ligand used to build up the electroactive multilayers are also described in the figure.

ADVANCED FUNCTIONAL MATERIALS



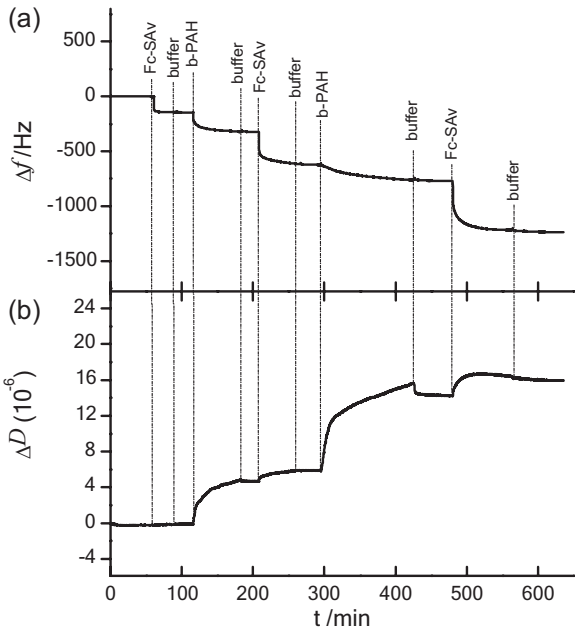


**Figure 2.** QCM response on a) frequency and b) dissipation at the overtone number $n = 7$ (35 MHz) describing the multilayer growth of the supramolecular assembly.

between solvent and solution can lead to significant changes in frequency and dissipation. In addition, physisorption (non-specific adsorption) of proteins onto the interfacial bioconjugate can lead to misleading interpretations of the actual frequency and dissipation changes corresponding to the bioconjugation of the protein onto the sensor surface. This is a very important observation that in many cases is not considered in the literature related to the QCM technique. In our case, rinsing with buffer did not promote any changes in frequency or dissipation, thus evidencing that the results were not influenced by the presence of non-specific adsorption and that the detected frequency and dissipation changes could be solely attributed to protein bioconjugation.

Then, the buffer solution was replaced by the b-PAH solution which was acting as a multivalent ligand[42,43] bioconjugating the Fc-SAv layer. In contrast to the first Fc-SAv layer, the recognition-mediated assembly of b-PAH displayed a slower decrease in frequency reaching a plateau after 50 min. Similarly, dissipation slowly increased during the conjugation of the b-PAH. The increase in energy dissipation is due to the nonrigid layer structure of b-PAH onto the Fc-SAv layer. Rinsing with buffer did not evidence any change in frequency and only slight changes in dissipation.

This clearly indicates that the entire biotinylated polymer that the QCM-D senses is conjugated to the Fc-SAv and no unbound polymer is present at the interface. On the other hand, the slight changes in dissipation could be attributed to relaxation or conformational changes of the b-PAH layer resulting in a more compact layer. Once rinsed, we assembled the second Fc-SAv layer onto the b-PAH layer. The initial exposure to the Fc-SAv solution leads to a rapid decrease in frequency followed by a slight steady decrease that reached the final plateau after 50 min. The assembly of the second layer of Fc-SAv only described a slight increase in dissipation, implying that the protein contributes to the dissipative characteristics of the interfacial architecture to a minor extent. Once again, the unperturbed value of the frequency obtained after rinsing demonstrates that the protein is firmly attached to the biotinylated polymer. This gives clear evidence that the multivalent character of b-PAH enables the creation of a biotinylated interface on top of the Fc-SAv layer where the upmost Fc-SAv is able to biorecognize the ligands without affecting the stability of the supramolecular architecture or the recognition properties of the protein. In close analogy to polyelectrolyte multilayers, where each polyion is responsible for the charge reversal of the interface,[44] the multivalent character of each building block is responsible for reversing the ligand/receptor character of the interface.

The conjugation of the second b-PAH layer is reflected as a very slow decrease in frequency. This could be attributed to conformational changes of the polymer chains during the conjugation. This macromolecular reorganization at the interface could lead to variations in trapped water, thus promoting viscoelastic changes that are sensed as a steady decrease in frequency. It is well known that viscoelastic changes in the interfacial architecture deposited on the sensor together with entrapment of water also contribute to the frequency shift during the measurement. This scenario is in agreement with the significant dissipation increase indicating that the $(\text{Fc-SAv})_2$ $(\text{b-PAH})_2$ assembly resembles a soft layer coupled viscoelatically to the gold-coated quartz crystal surface.

After rinsing, the assembly of the third Fc-SAv layer was accomplished. This led to a significant decrease in frequency accompanied by an increase in dissipation. Rising with buffer demonstrated that the redox-active protein was efficiently anchored to the supramolecular architecture and no weakly bound proteins were at the sensor surface.

The results indicate that by increasing the number of layers the viscoelastic characteristics of the interfacial architecture are increased. As an attempt to observe the evolution of the film properties during the multilayer growth we followed the sequential layer-by-layer bioconjugation at different overtones. In accordance to the Sauerbrey equation,[45]

$$\Delta m = -\frac{C\,\Delta f}{n} \tag{1}$$

where $\Delta f$ is the change in frequency, $\Delta m$ is the change in mass, $n$ is the overtone number, and $C$ is the mass sensitivity constant.

This would indicate $\Delta f$ scales with $n$ in case of having a rigid film described by the Sauerbrey equation. Strictly speaking this is valid only for uniform rigid films with material properties indistinguishable from those of the crystal resonator. Obviously, this is not the case of soft matter-based architectures attached to the resonator in a liquid environment. Even if the layer is firmly attached, the retained water is not strictly "fixed" to the film. In our case, the solvent is hydrodynamically

  

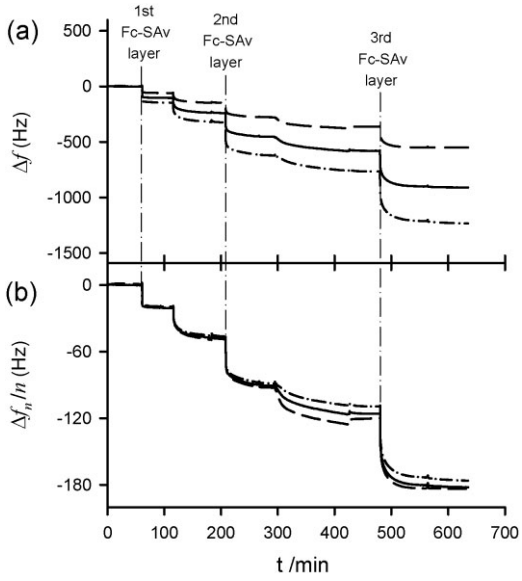


**Figure 3.** a) Representation of frequency ($\Delta f$) and b) normalized frequency ($\Delta f/n$) at different overtones obtained during the multilayer growth. The different overtones correspond to: (dashed line) $n = 3.15$ MHz; (solid line) $n = 5$, 25 MHz; (dash-dotted line) $n = 7$, 35 MHz.

coupled to the supramolecular assembly. However, in some cases dealing with soft matter the mechanical properties of the film resembles those of a rigid layer in the sense of the Sauerbrey equation. Recently, Notley et al. reported that the parameter $\Delta f/n$ in the growth of polyelectrolyte multilayers is independent of frequency throughout the assembly, indicating that the film is rigid enough to use the Sauerbrey equation as a first approximation.[46] In a similar fashion, we propose analyzing $\Delta f/n$ at different overtones as a strategy to obtain information of the multilayer growth. It is worth mentioning that we do not attempt to carry out a quantitative measurement of the mass coverage using the Sauerbrey equation. Our goal is to explore the variation in rigidity/softness at different growth stages by simply studying the departure from the Sauerbrey scaling.[45]

Figure 3 shows the plots $\Delta f_n$ versus time obtained at $n = 3$, $n = 5$, and $n = 7$ normalized by the overtone number. As a result, we observed a Sauerbreyian response ($\Delta f_n/n = \text{constant}$) only in the early stages of growth. Beyond the first (Fc-SAv)/(b-PAH) bilayer, the interfacial architecture becomes less rigid and more dissipative, probably due to the significant amount of water trapped into the film.

The different structural characteristics of the supramolecular assembly at different growth stages are also evidenced by atomic force microscopy (AFM). Topographic imaging of the supramolecular assembly reveals a clear roughness evolution upon multilayer growth (Fig. 4).

AFM imaging on the biotinylated Au surface evidenced changes on the topography after bioconjugating the first Fc-SAv layer. The presence of the protein led to a homogenously distributed nodular-like film deposited on the surface. The assembly of b-PAH onto the Fc-SAv also revealed a corrugated film with a similar nodular-like structure (RMS: 0.5 nm). The incorporation of b-PAH did not significantly contribute to the roughness of the film (RMS: 0.5 nm). However, the sequential incorporation of layers leads to a roughness increase, as derived from the roughness values of 0.9 nm for the $(\text{Fc-SAv})_3(\text{b-PAH})_2$.

The multilayer growth of the supramolecular assembly was also characterized by surface plasmon spectroscopy (SPR). Figure 5 shows the different reflectivity curves obtained during the layer-by-layer growth of Fc-SAv mediated by the polyvalent anchoring of b-PAH. SPR response originates from refractive index changes as water is replaced by the biomolecules and the shifts in the minimum of the angular $\theta$-scans of reflected intensity ($\Delta\theta$) are reflecting the sequential assembly of the different building blocks into the interfacial architecture. These reflectivity shifts can also be correlated to thickness values. In our case, from $\Delta\theta$ values we estimated 6 nm as the total thickness of the $(\text{Fc-SAv})_3(\text{b-PAH})_2$ assembly used in this work.

### 2.2. Unidirectional Electron Transfer in Redox-active Supramolecular Bioconjugates

The electroactivity of the supramolecular assemblies was studied by cyclic voltammetry. Figure 6 shows the cyclic voltammograms corresponding to $(\text{Fc-SAv})_n(\text{b-PAH})_{n-1}$ supramolecular bioconjugates with different number of redox-active multilayers ($n = 1,2$, and 3). As expected, the increasing number of Fc-SAv layers incorporated into the assembly is reflected in higher charge values associated to the oxidation–reduction of the ferrocene centers linked to the

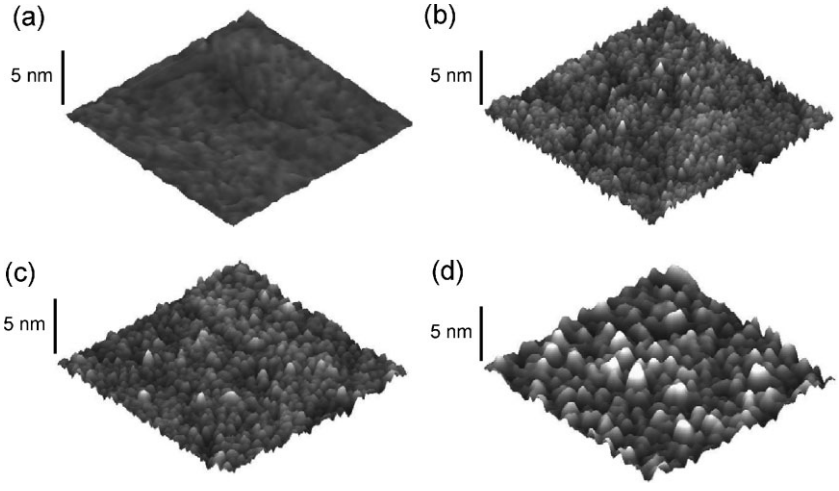


**Figure 4.** AFM topographic imaging ($500 \times 500\ \text{nm}^2$) corresponding to: a) biotinylated gold electrode, b) Fc-SAv-modified Au electrode, c) (Fc-SAv)(b-PAH)-modified Au electrode, and d) $(\text{Fc-SAv})_3(\text{b-PAH})_2$-modified Au electrode.

ADVANCED FUNCTIONAL MATERIALS



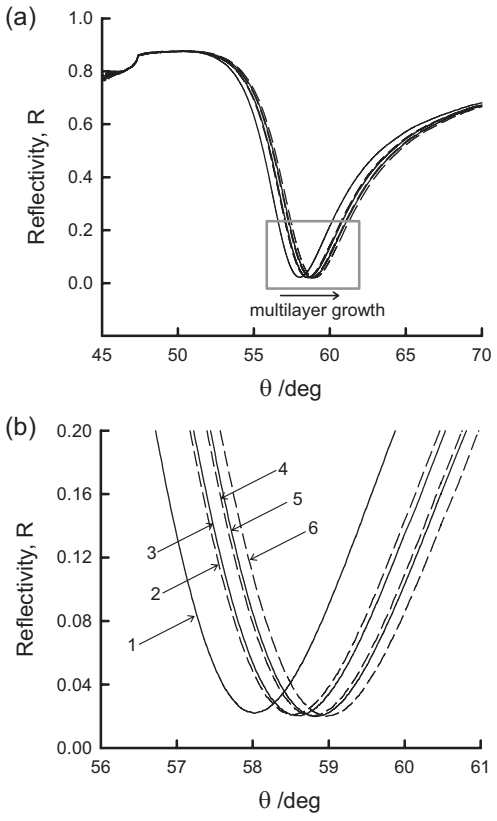


**Figure 5.** a) Reflected intensity as a function of the angle-of-incidence scan ($\theta$) plot describing the supramolecular assembly of the multilayered structure on the Au electrode. The reflectivity shifts are evidencing the sequential assembly of the different molecular building blocks into the interfacial architecture. b) Expanded view of the SPR minimum part indicated with a gray frame in panel a). The different reflectivity curves correspond to: 1) biotinylated Au surface, 2) Fc-SAv, 3) (Fc-SAv)(b-PAH), 4) $(Fc\text{-}SAv)_2$(b-PAH), 5) $(Fc\text{-}SAv)_2(b\text{-}PAH)_2$, and 6) $(Fc\text{-}SAv)_3(b\text{-}PAH)_2$.

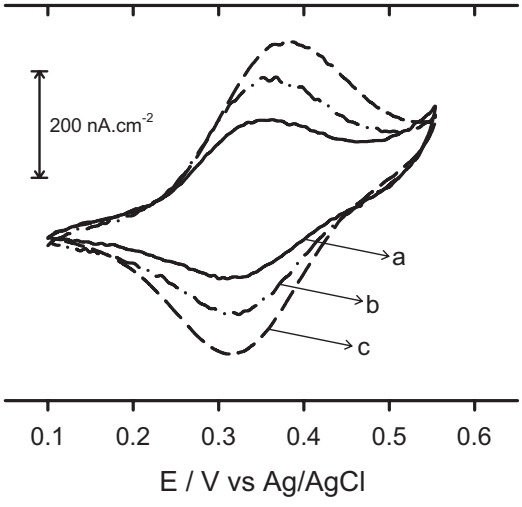


**Figure 6.** Cyclic voltammograms corresponding to the different supramolecular multilayered assemblies conjugated onto the Au electrode: a) Fc-SAv, b) $(FcSAv)_2$(b-PAH), c) $(Fc\text{-}SAv)_3(b\text{-}PAH)_2$. The voltammograms are depicted in different traces for the sake of clarity. $\nu = 20$ mV $s^{-1}$. T = 298 K. Electrolyte: 0.1 M PBS solution

**Table 1.** Details of the charge and coverage of redox centers and proteins associated to the different supramolecular architectures.

| Interfacial Architecture | Charge [$\mu$C $cm^{-2}$] | Population of ferrocene sites [Fc molec $cm^{-2}$] | Electrochemical estimation of SAv in the bioconjugate [SAv molec $cm^{-2}$] |
|---|---|---|---|
| (Fc-SAv) | $1.3 \pm 0.3$ | $8 \times 10^{12}$ | $2 \times 10^{12}$ |
| $(Fc\text{-}SAv)_2$(b-PAH) | $2.8 \pm 0.2$ | $1.7 \times 10^{13}$ | $4.2 \times 10^{12}$ |
| $(Fc\text{-}SAv)_3(b\text{-}PAH)_2$ | $4.0 \pm 0.3$ | $2.5 \times 10^{13}$ | $6.2 \times 10^{12}$ |

streptavidins. Taking into account that each Fc-SAv molecule carries four ferrocene units we obtained an electrochemical estimate of the protein coverage incorporated on each assembly step (Table 1). Considering that one full monolayer of SAv bioconjugated on a biotin-terminated surface is constituted of $2.1 \times 10^{12}$ molec $cm^{-2}$[47] (which is equivalent to 210 ng $cm^{-2}$) we could infer that in the sequential multilayer growth we were incorporating nearly one Fc-SAv monolayer per protein conjugation step (Table 1).

The good reversibility of the voltammetric response[48,49] corresponding to the ferrocene labels incorporated into bioconjugate layer is a clear indication that the electron transfer across the redox-active interfacial architecture is completely feasible. This implies that, in spite of the complexity of the interfacial supramolecular architecture, the ferrocene labels are "wired" through the supramolecular array to the Au electrode.

To further characterize the electroactive behaviour of the redox-labeled assembly we proceeded to study the dependence of the current peaks ($j_p$) with the scan rate ($\nu$). The dependence of $j_p$ on $\nu$ can provide powerful insight on the mechanisms governing the redox characteristics of the supramolecular assembly.[50] In general terms, an ideally responding surface-confined redox species is described by a linear correspondence between $j_p$ on $\nu$.[48] Conversely, when diffusional charge transport through the electroactive film starts to operate $j_p$ increases as $\nu^{0.5}$.[50] In our case, Figure 7 displays the variation of the anodic $j_p$ with $\nu$ for the different multilayered assemblies: Fc-SAv, $(FcSAv)_2$(b-PAH), and $(Fc\text{-}SAv)_3(b\text{-}PAH)_2$. It can be observed that the linear correspondence between $j_p$ on $\nu$ is only satisfied by the Fc-SAv architecture whereas $(FcSAv)_2$(b-PAH) and $(Fc\text{-}SAv)_3(b\text{-}PAH)_2$ fail to describe a linear $j_p$ versus $\nu$ correspondence (Fig. 7a). On the other hand, the scaling of $j_p$ with $\nu^{0.5}$ for the $(FcSAv)_2$(b-PAH) and $(Fc\text{-}SAv)_3(b\text{-}PAH)_2$ architectures described a very good linear relationship and, as expected, Fc-SAv did not follow a linear correspondence with $\nu^{0.5}$ (Fig. 7b). These results clearly indicate that Fc-SAv behaves as a typical electroactive film containing surface-confined redox centers and, in contrast, $(FcSAv)_2$(b-PAH) and $(Fc\text{-}SAv)_3(b\text{-}PAH)_2$ assemblies display characteristics corresponding to electroactivity governed by diffusional charge transport through the supramolecularly assembled film. This can be explained considering that, in many cases, electrochemical charge transport through multilayered films occurs by electron self-exchange between neighboring oxidized and reduced centers.[50] In addition, this electron–hopping process

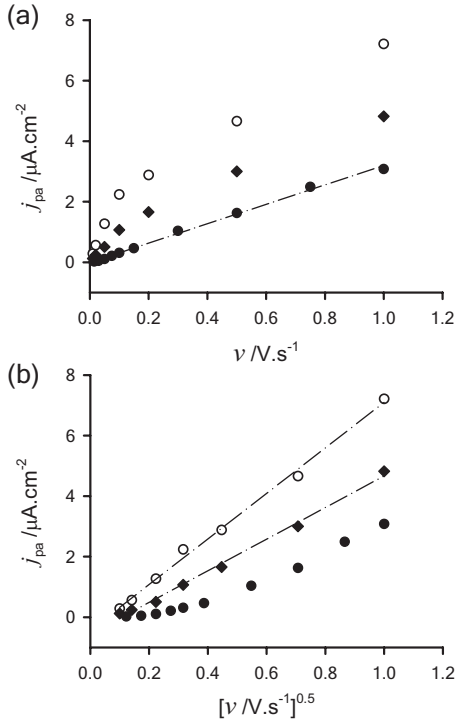


**Figure 7.** Plots describing the dependence of the anodic peak current density ($j_{pa}$) on the scan rate ($\nu$): a) $j_{pa}$ versus $\nu$ and b) $j_{pa}$ versus $\nu^{0.5}$. The different symbols correspond to: (●) Fc-SAv, (◆)(FcSAv)$_2$(b-PAH), and (○) (Fc-SAv)$_3$(b-PAH)$_2$. The straight dashed lines are introduced for guiding the eye.

is also accompanied by the movement of charge-compensating counterions that are mobile within the assembled layer. Consequently, the diffusional characteristics of the charge transport of the (FcSAv)$_2$(b-PAH) and (Fc-SAv)$_3$(b-PAH)$_2$ assemblies could be ascribed to the ''diffusion'' of either electrons or charge-compensating counterions through the supramolecularly assembled film.[51]

One important aspect related to the use of these redox-active assemblies as building blocks in bioelectronics lies in the fact that the chemical/electrochemical state of these ferrocene redox sites can be easily controlled by the electrode potential. Tuning the Fermi level of the metal electrode (by controlling the electrode potential) enables the electron transfer between the metal electrode and the redox labels to be manipulated. This means that turning the ferrocene moieties into ferricinium species is a straightforward step easily triggered by the electrode potential. The presence of electron donors in the solution interacting with the electrogenerated ferricinium sites would lead to their oxidation by electron exchange with oxidized sites (acceptor species) in the supramolecular assembly.[13] This implies that the electronic readout of the whole electron transfer process should be an anodic current.[52–54] On the other hand, if the reverse reaction is thermodynamically restricted or the transport of acceptors to the Au electrode is hindered,[55] the charge transfer process across supramolecular architecture would not be possible. As a consequence, the electronic readout would indicate no current flow across the bio-assembled interface. This is the basic principle of the rectification by an electrochemical diode.[52–54]

Typically, that is the case if electron acceptors in solution, like $[Fe(CN)_6]^{4-}$ species, interact with reduced ferrocene sites in the interfacial assembly. $[Fe(CN)_6]^{4-}$ species have a less noble character ($E^o = 0.358$ V) compared with Fc species ($E^o = 0.400$ V). This indicates that the spontaneous reduction of ferricenium to ferrocene in the presence of ferrocyanide is a thermodynamically favorable process. In contrast, the magnitude of the redox potentials indicates that the ferrocene centers will not oxidize in contact with ferricyanide because of being a thermodynamically restricted process. Consequently, no cathodic current is expected upon reversing the scan in the cathodic direction.[13]

Figure 8 shows the voltammetric response of a single-layer Fc-SAv assembly conjugated on the Au electrode in the presence of 3 mM $Fe(CN)_6^{4-}$. The electrochemical rectification is evidenced as a notorious anodic peak, while no cathodic peak is observed in the voltammetric cycle. The anodic current peak originates from $Fe(CN)_6^{4-}$ oxidation mediated by the Fc/Fc$^+$ species confined to the redox-active supramolecular assembly. As previously discussed, the absence of a cathodic signal after reversing the potential scan should be attributed to the fact that the electrogenerated ferrocene is not strong enough to reduce the ferricyanide, hence there is no electron exchange. This scenario resembles the generation of electrocatalytic currents originated from the mediation of surface-confined redox centers in the presence of redox species in solution. That is why the rectified electrochemical currents are commonly referred to as electrocatalytic currents ($j_{ecat}$).[13]

One of the key advantages of using redox-active supramolecular bioassemblies to control the unidirectional electron transfer lies in the versatility to design interfaces manipulating the incorporation of redox functionalities through molecular recognition processes (Fig. 9). This is a feature of major relevance that implies creating chemical strategies to tune and amplify the electronic readout in a controlled manner.

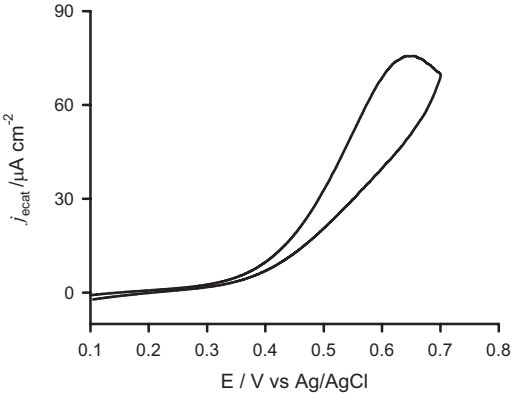


**Figure 8.** Cyclic voltammogram describing the electrochemical rectification observed at a Fc-SAv-modified Au electrode in the presence of $Fe(CN)_6^{4-}$ (electron donor) species in solution. $\nu = 50$ mV s$^{-1}$. T = 298 K. Electrolyte: 3 mM $Fe(CN)_6^{4-}$ (in 0.1 M PBS solution).

ADVANCED FUNCTIONAL MATERIALS



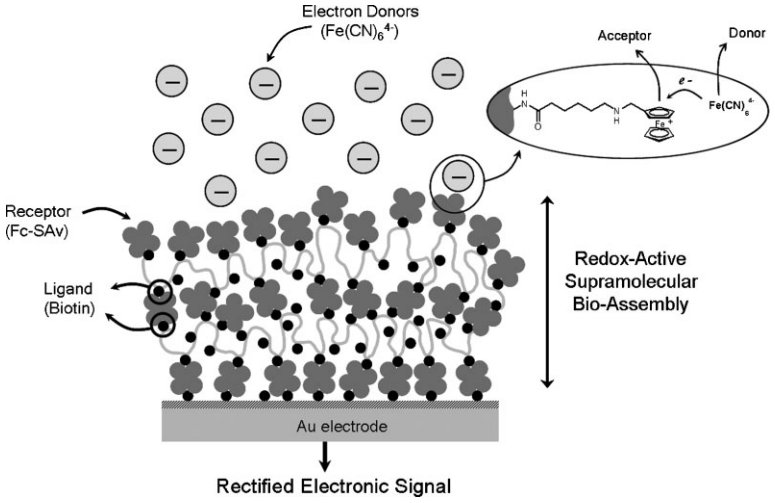


**Figure 9.** Simplified scheme describing the different building blocks and chemical species involved in the generation of the rectified electronic signal.

Different research groups have described the current generated at an electrode containing surface-confined redox sites undergoing bimolecular electron transfer reactions with electron donor/acceptors in solution, i.e., electrochemical rectification.[13,56–59] In that case the rectified current density ($j$) is given by

$$j = F\, k_{\text{cross}} \Gamma_o c_D \qquad (2)$$

where $F$ is the Faraday constant, $k_{\text{cross}}$ the rate constant for the bimolecular reaction between electron donors and acceptors, $\Gamma_o$ is the coverage of redox-active sites, and $c_D$ is the concentration of donor (or acceptor) species in solution. From Eq. (2) it is clear that the magnitude of the rectified current can be tuned through two adjustable chemical parameters. One of them, the population of redox sites in the interfacial architecture, depends exclusively on the design of the multilayered redox assembly. Increasing the number of redox-active proteins into the conjugate layer would impact on a further amplification of the rectified electronic readout. The other parameter, the concentration of $Fe(CN)_6^{4-}$ (electron donors) in solution is another variable that can be easily tuned to set the magnitude of the rectified current.

Figure 10a displays the changes in the rectified electronic readout upon increasing the number of Fc-SAv bioconjugated to the supramolecular assembly if the electrode is exposed to 5 mM $Fe(CN)_6^{4-}$. It can be clearly seen that, as expected, increasing the number of Fc-SAv layers impacts on higher rectified currents.

Changing from one Fc-SAv layer to two and three Fc-SAv layers is reflected as a rectified current increase from 177 to 360 and 552 μA $cm^{-2}$, respectively. This implies that when the $(Fc\text{-}SAv)_3(b\text{-}PAH)_2$ interfacial architecture is polarized at 0.7 V (vs. Ag/AgCl) in the presence of 5 mM $Fe(CN)_6^{4-}$ a unidirectional current flow equivalent to 552 μA $cm^{-2}$ develops through the metal electrode. And then, when the polarization is reversed to 0.1 V (vs. Ag/AgCl) no current flow through the interface is detected. This example would provide an estimation of the current densities that the bio-assembled interface could support when implemented in a device. A quantitative increase in current with the number of Fc-SAv layers is in full agreement with the increased number of mediators (ferrocene sites) in the bioconjugate structure. In is worth noticing that in case the bimolecular reaction occurs exclusively at the topmost layer of the bioconjugate the electronic readout would not be so sensitive to the variation in the population of redox sites. In contrast, these results would imply that the bimolecular electron transfer reaction between the confined Fc sites and $Fe(CN)_6^{4-}$ occurs across the whole bioconjugate structure. The very soft character of

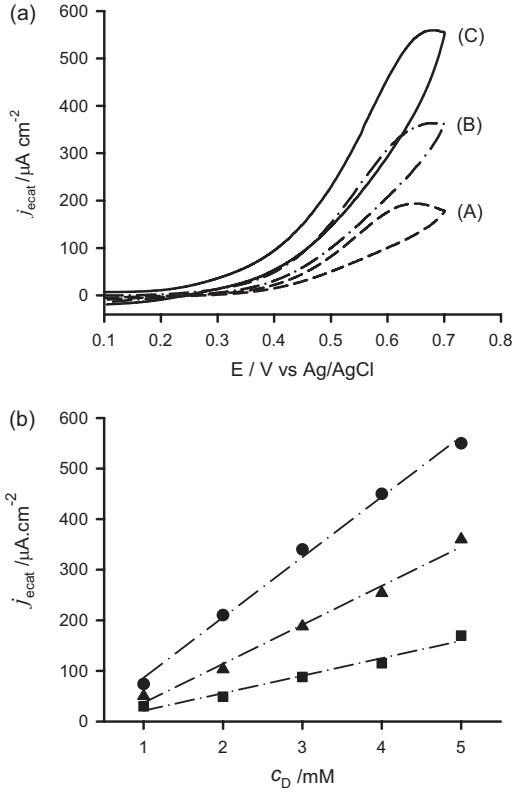


**Figure 10.** a) Cyclic voltammograms displaying the current rectification at a Au electrode bioconjugated with different supramolecular multilayered assemblies: A) Fc-SAv, B) $(FcSAv)_2(b\text{-}PAH)$, C) $(Fc\text{-}SAv)_3(b\text{-}PAH)_2$. The voltammograms are depicted in different traces for the sake of clarity. $\nu = 50$ mV $s^{-1}$. T = 298 K. Electrolyte: 5 mM $Fe(CN)_6^{4-}$ + 0.1 M PBS solution. b) Representation of the electrocatalytic (rectified) current as a function of the concentration of donor species, $c_D$ ($Fe(CN)_6^{4-}$), in solution for the different supramolecular assemblies: (■) Fc-SAv, (▲) $(FcSAv)_2(b\text{-}PAH)$, (●) $(Fc\text{-}SAv)_3(b\text{-}PAH)_2$.

the interfacial architecture containing trapped electrolyte solution would facilitate the transport of $Fe(CN)_6^{4-}$ species to the inner environment of bioconjugate, thus explaining the quantitative amplification upon increasing the number of Fc-SAv layers.

In order to further analyze this scenario we studied the variation of the rectified current with increase in concentrations of donors in solution. Figure 10b describes linear $j_{ecat}$ versus $c_D$ plots for different assemblies containing increasing amounts of Fc-SAv layers. This experimental observation is in agreement with that predicted by Eq. (2) considering that in any case the coverage of redox sites remains constant. Moreover, Eq. (2) also predicts that the sensitivity of the amplified readout (slope of $j_{ecat}$ vs. $c_D$ plot) is dependent on the amount of redox sites involved in the bimolecular reaction. As can be seen in Figure 10b the slope of the different $j_{ecat}$ versus $c_D$ plots is sensitive to the number of Fc-SAv layers in the bioconjugate, thus demonstrating that the amplification of the rectified signal is sensitively affected by the number of building blocks constituting the multilayered assembly.

The sensitivities of the interfacial architectures Fc-SAv, $(Fc\text{-}SAv)_2(b\text{-}PAH)_1$, and $(Fc\text{-}SAv)_3(b\text{-}PAH)_2$ corresponded to 35, 76, and 115 $\mu A\ cm^{-2}\ mM^{-1}$, respectively. These sensitivity values are in excellent agreement with the expected ones if we consider that all the redox centers in the bioconjugate participate. Assuming that $k_{cross}$ solely depends on the interacting Fc and $Fe(CN)_6^{4-}$ species and the interfacial architecture has no influence on its value, from Eq. (2) we can infer that the sensitivity of the rectifying assembly is directly correlated to the electrochemical charge of the assembly. In other words, increasing $n$ times the electrochemical charge will impact on an $n$-fold increase in sensitivity.

This correlation is illustrated in Figure 11 in which the experimental sensitivities are represented together with the "expected" sensitivities derived from Eq. (2) and assuming that all the ferrocene centers are involved in the bimolecular reaction. The excellent agreement between both values strongly suggests that, in fact, all the electroactive centers incorporated into the bioconjugate participate in the redox mediation and are responsible for tuning the electron transfer across the interfacial architecture.

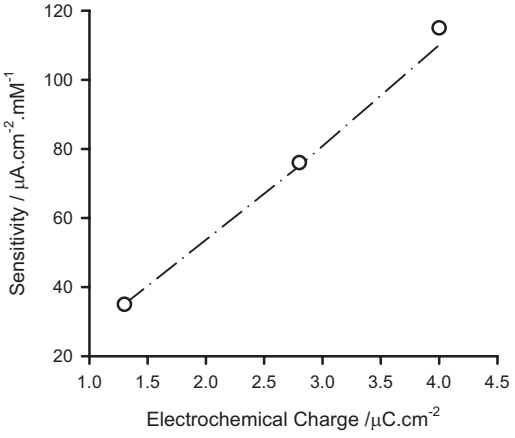


**Figure 11.** Representation of the sensitivity of the rectifying bioelectrochemical device versus the electrochemical charge associated to the oxidation–reduction of the ferrocene centers incorporated into the supramolecular assembly. The dotted line represents the theoretical sensitivity assuming that the whole population of electroactive centers into the assembly participate in the bimolecular donor/acceptor electron transfer reaction [cf. Eq. (2)]. The empty circles represent the experimental values.

## 3. Conclusions and Outlook

In this work, we have described a new strategy to build-up electroactive molecular platforms suitable for creating molecular rectifiers. This approach was based on the use of ferrocene-labeled streptavidin molecules as electroactive bioinorganic building blocks displaying molecular–recognition properties. These building blocks were assembled onto the metal electrode by strong ligand/receptor biological interactions using multivalent macromolecular ligands as scaffolds for building-up multilayered structures. The very specific interactions between biotin and SAv were responsible for conferring stability to the supramolecular interfacial architecture. Even though the multilayer assembly resembles a quite complex and intrincate supramolecular system, the experimental evidence demonstrated the feasibility of transferring charge across the bioconjugate. This means that the complexity of the supramolecular assembly does not affect the connectivity between the redox centers incorporated in the bioconjugate layer and the metal electrode. Locally addressing the redox centers within the supramolecular assemblies represented the structural and functional basis for the design of a molecular device. This was demonstrated through the creation of different mulilayered interfacial architectures held together by strong non-covalent interactions incorporating redox functionalities in a topologically controlled manner.

These redox-active interfacial architectures were successfully used for mediating and rectifying the electron transfer between redox donors in solution and the Au electrode. Interestingly, our experimental results indicated that the whole population of redox centers incorporated within the assembly participate in the bimolecular electron–transfer reaction leading to the electrochemical rectification. This could be attributed to the trapping of significant amounts of electrolyte by the soft interfacial architecture, which enables the transport of donor species in solution to the different redox sites in the inner environment of the supramolecular bioconjugate. Accordingly, this bio-supramolecular approach enabled the generation of interfacial architectures displaying tunable unidirectional current flow. The versatility of supramolecular chemistry using biological interactions provided the pathway to incorporate into the molecular assembly in a controlled manner electron acceptors communicating with the metal electrode. These electron acceptors together with electron donors in solution are responsible for tuning the amplification of the electronic readout corresponding to the unidirectional

ADVANCED FUNCTIONAL MATERIALS



electron transfer, thus acting as a tunable bio-supramolecular diode.

These results using redox-active supramolecular assemblies demonstrate the potential of using molecular recognition-directed assembly in combination with hybrid bio-inorganic building blocks to create multifunctional interfacial architectures. This approach would enable to locally address the redox centers within the supramolecular assembly with molecular precision, representing a crucial feature for the design of molecular devices. We envision that this strategy exploiting the properties of self-organizing systems would provide a new class of hybrid materials displaying pre-designed functionalities at controlled sites into 3D interfacial nanoarchitectures built-up by bottom-up approaches.

## 4. Experimental

*Materials*: Streptavidin, potassium ferrocyanide, phosphate buffered saline (PBS), *N*-hydroxysuccinimide (NHS), dimethylformamide (DMF), [*N*-(3-dimethylaminopropyl)-*N*′-ethyl-carbodiimide-hydrochloride] (EDC), 11-mercaptoundecanol, poly(allylamine) were purchased from Sigma–Aldrich. Biotin-terminated thiol [**1**,12-mercaptododecanoic-(8-biotinoylamido-3,6-dioxaoctyl)amide] was obtained from Boeringer Mannheim. [*N*-(ferrocenylmethyl)-6-amino] hexanoic acid was synthesized as previously described in the literature [60].

*Synthesis of Ferrocene-labeled Streptavidin (Fc-SAv)*: The redox-labeled protein was synthesized at the Max-Planck-Institut für Polymerforschung following procedures reported in the literature.[61,62] Briefly, [*N*-(ferrocenylmethyl)-6-amino]hexanoic acid (30 mg, 91 mmol), NHS (11 mg, 96 mmol), and [*N*-(3-dimethylaminopropyl)-EDC] (18 mg, 94 mmol) in 0.5 mL of dry DMF were heated under $N_2$ amosphere and stirring at 80 °C for 30 min. Aliquots ($5 \times 10$ μL) of these solution were added to added at room temperature to a solution of 1 mg of streptavidin in 0.5 mL phosphate buffer (0.1 M, pH 8.5). To remove unreacted ferrocene, the solution of the modified streptavidin was extensively dialyzed against PBS buffer (0.05 M, pH 7.4) [61,62]. The spectrophotometrically determined Fc/SAv ratio was ~4. The biotin binding capacity of Fc-SAv was determined SPR and was found to be similar to SAv [61].

*Synthesis of Biotinylated poly(allylamine)hydrochloride*: 6-Biotinyl-NHS ester (0.41 g, $1.26 \cdot 10^{-3}$ mol) [63] was dissolved in 3 mL DMF by heating up to 80 °C. The solution was cooled to room temperature and was added dropwise to a solution of 0.5 g of PAH (MW ~ 15 000) solution in 3 mL aqueous PBS buffer containing 0.13 g of $NaHCO_3$ ($1.575 \cdot 10^{-3}$ mol, 1.5 equivalent of biotin-NHS). The clear solution obtained was allowed to stir at room temperature for 24 h and subjected to dialysis against water during 5 days (dialysis membrane cut-off was 3500). The aqueous solution was lyophilized to give biotinylated poly(allylamine) hydrochloride (b-PAH) as white solid. The content of biotin was determined by $^1$H-NMR and was found to be 21%.

*Electrochemical Measurements*: Cyclic voltammetry experiments were performed with an Autolab potentiostat using a conventional three-electrode cell equipped with a Ag/AgCl reference electrode and a graphite counter electrode.

*Surface Plasmon Resonance*: SPR detection was carried out in a home-made device under a Kretschmann configuration [64]. A thin Au film (50 nm) was evaporated on the surface of LaSFN9 glass plates (produced by Schott Glass GmbH, $n = 1.85$ at $\lambda = 633$ nm). It was then optically matched to the base of a 90 ° LaSFN9 glass prism. The surface plasmons were excited at the metal/dielectric interface upon total internal reflection of laser beam (HeNe, $\lambda = 632.8$ nm, power = 5 mW) at the prim base. By varying the angle of incidence the reflected light showed a sharp minimum at a resonance angle which is dependent upon the precise architecture of the metal/dielectric interface (scan mode). From the Fresnel fit to the resonance curve of bare and layer-coated Au surfaces it was possible to obtain the thickness and dielectric constant of the sample layers. The addition of a thin layer to the surface of the Au typically shifted the position of the resonance to a higher angle. Fitting those subsequent curves determined the optical thickness of the layer. The accurate conversion of the optical thickness to the geometrical thickness requires the knowledge of the refractive index of the films, which is a parameter dependent on the molecular composition of the film and the packing density. We assumed a value $n = 1.5$ for all deposited materials [65,66].

*Quartz Crystal Microbalance with Dissipation Monitoring*: The QCM-D measurements were carried out at 21 °C using a Q-Sense microbalance (Q-Sense, Göteborg, Sweden). This instrument allows for a simultaneous measurement of frequency change ($\Delta f$) and energy dissipation change ($\Delta D$) by periodically switching off the driving power of the oscillation of the sensor crystal and by recording the decay of the damped oscillation. The time constant of the decay is inversely proportional to $D$, and the period of the decaying signal gives $f$. Experiments were performed using commercially available (QSX-301, Q-Sense) gold-coated quartz crystals.

*Atomic Force Microscopy*: Images were taken in air at room temperature with a commercial AFM Dimension 3000 (Veeco) controlled with a Nanoscope V, operating in tapping mode. Silicon cantilevers (Olympus) 160 μm long, 50 μm wide, and 4.6 μm thick, with an integrated tip of a nominal spring constant of 42 N $m^{-1}$ and a resonance frequency of 300 kHz were used. In a typical experiment, the tip was scanned at velocity in the range 0.8–1 Hz and minimal applied forces were used when imaging. Topography and phase images were used to record the structures.

Received: June 4, 2008
Revised: July 17, 2008
Published online: October 17, 2008

[1] V. Heleg-Shabtai, T. Gabriel, I. Willner, *J. Am. Chem. Soc.* **1999**, *121*, 3220.
[2] M. C. Lonergan, *Science* **1997**, *278*, 2103.
[3] *Biophysics of Electron Transfer and Molecular Bioelectronics* (Ed: C. Nicolini), Springer, Heidelberg **1999**.
[4] D. K. James, J. M. Tour, in *Nanoscale Assembly: Chemical Techniques* (Ed: W. T. S. Huck), Springer, Heidelberg **2005**, Ch. 5, pp. 79–98.
[5] *Bioelectronics: From Theory to Applications* (Eds: I. Willner, E. Katz), VCH-Wiley, Weinheim **2005**.
[6] V. Balzani, A. Credi, M. Venturi, *Chem. Eur. J.* **2008**, *14*, 26.
[7] A. N. Shipway, I. Willner, *Acc. Chem. Res.* **2001**, *34*, 421.
[8] E. Gomar-Nadal, J. Puigmartí-Luis, D. B. Amabilino, *Chem. Soc. Rev.* **2008**, *37*, 490.
[9] M. Ruben, J.-M. Lehn, P. Muller, *Chem. Soc. Rev.* **2006**, *35*, 1056.
[10] W. Wang, T. Lee, M. A. Reed, in *Nanoscale Assembly: Chemical Techniques* (Ed: W. T. S. Huck), Springer, Heidelberg **2005**, Ch. 3, pp. 43–64.
[11] B. Mukherjee, K. Mohanta, A. J. Pal, *Chem. Mater.* **2006**, *18*, 3302.
[12] J. W. Baldwin, R. R. Amaresh, I. R. Peterson, W. J. Shumate, M. P. Cava, M. A. Amiri, R. Hamilton, G. J. Ashwell, R. M. Metzger, *J. Phys. Chem. B.* **2002**, *106*, 12158.
[13] K. S. Alleman, K. Weber, S. E. Creager, *J. Phys. Chem.* **1996**, *100*, 17050.
[14] S. I. Stupp, M. Kesser, G. N. Tew, *Polymer* **1998**, *39*, 4505.
[15] G. N. Tew, M. U. Pralle, S. I. Stupp, *Angew. Chem, Int. Ed.* **2000**, *39*, 517.
[16] T. Bein, *Supramolecular Architecture: Synthetic Control in Thin Films and Solids* (Ed: T. Bein), American Chemical Society, Washington **1992**, Ch. 1, pp. 1–7.

  

[17] V. M. Rotello, *Curr. Org. Chem.* **2001**, *5*, 1079.
[18] A. Verma, V. M. Rotello, *Chem. Comm.* **2005**, 303.
[19] J. J. Davis, *Chem. Comm.* **2005**, 3509.
[20] R. Shenhar, V. M. Rotello, *Acc. Chem. Res.* **2003**, *36*, 549.
[21] S. Srivastasa, A. Verma, B. L. Frankamp, V. M. Rotello, *Adv. Mater.* **2005**, *17*, 617.
[22] R. Shenhar, A. Sanyal, O. Uzun, H. Nakade, V. M. Rotello, *Macromolecules* **2004**, *37*, 4931.
[23] O. Crespo-Biel, B. Dordi, D. N. Reinhoudt, J. Huskens, *J. Am. Chem. Soc.* **2005**, *127*, 7594.
[24] M. Ahlers, W. Muller, A. Reichert, H. Ringsdorf, J. Venzmer, *Angew. Chem, Int. Ed.* **1990**, *29*, 1269.
[25] C. M. Niemeyer, in *Nanobiotechnology: Concepts, Applications and Perspectives* (Eds: C. M. Niemeyer, C. A. Mirkin), Wiley-VCH, Weinheim **2004**, Ch. 15, pp. 227–243.
[26] A. Mulder, J. Huskens, D. N. Reinhoudt, *Org. Biol. Chem.* **2004**, *2*, 3404.
[27] O. Crespo-Biel, B. J. Ravoo, D. N. Reinhoudt, J. Huskens, *J. Mater. Chem.* **2006**, *16*, 3997.
[28] R. S. Kane, *AlChE J.* **2006**, *52*, 3638.
[29] L. L. Kiessling, J. E. Gestwicki, L. E. Strong, *Angew. Chem, Int. Ed.* **2006**, *45*, 2348.
[30] P. R. Rai, A. Saraph, R. Ashton, V. Poon, J. Mogridge, R. S. Kane, *Angew. Chem, Int. Ed.* **2007**, *46*, 2207.
[31] M. Mammen, S.-K. Choi, G. M. Whitesides, *Angew. Chem, Int. Ed.* **1998**, *37*, 2754.
[32] J.-i. Anzai, Y. Kobayashi, N. Nakamura, M. Nishimura, T. Hoshi, *Langmuir* **1999**, *15*, 221.
[33] T. Cassier, K. Lowack, G. Decher, *Supramol. Sci.* **1998**, *5*, 309.
[34] S. Lindegren, H. Andersson, L. Jacobsson, T. Back, G. Skarnemark, B. Karlsson, *Bioconjugate Chem.* **2002**, *13*, 502.
[35] N. Kato, F. Caruso, *J. Phys. Chem. B* **2005**, *109*, 19604.
[36] Z. Dai, J. T. Wilson, E. L. Chaikof, *Mater. Sci. Eng C* **2007**, *27*, 402.
[37] J.-i. Anzai, M. Nishimura, *J. Chem. Soc. Perkin Trans.* **1997**, *2*, 1887.
[38] J. Spinke, M. Liley, F.-J. Schmitt, H.-J. Guder, L. Angermaier, W. Knoll, *J. Chem. Phys.* **1993**, *99*, 7012.
[39] V. H. Pérez-Luna, M. J. O'Brien, K. A. Opperman, P. D. Hampton, G. P. López, L. A. Klumb, P. S. Stayton, *J. Am. Chem. Soc.* **1999**, *121*, 6469.
[40] K. E. Nelson, L. Gamble, L. S. Jung, M. S. Boek, E. Naeemi, S. L. Golledge, T. Sasaki, D. G. Castner, C. T. Campbell, P. S. Stayton, *Langmuir* **2001**, *17*, 2807.
[41] L. S. Jung, K. E. Nelson, P. S. Stayton, C. T. Campbell, *Langmuir* **2000**, *16*, 9421.
[42] G. Thoma, M. B. Streiff, A. G. Katopodis, R. O. Duthaler, N. H. Voelcker, C. Ehrhardt, C. Masson, *Chem. Eur. J.* **2006**, *12*, 99.
[43] D. A. Fulton, S. J. Cantrill, J. F. Stoddart, *J. Org. Chem.* **2002**, *67*, 7968.
[44] G. Decher, in *Multilayer Thin Films: Sequential Assembly of Nanocomposite Materials* (Eds: G. Decher, J. B. Schlenoff), Wiley-VCH, Weinheim **2002**, Ch. 1, pp. 1–46.
[45] G. Sauerbrey, *Z. Phys.* **1959**, *155*, 206.
[46] S. M. Notley, M. Eriksson, L. Wagberg, *J. Colloid. Interface Sci.* **2005**, *292*, 29.
[47] O. Azzaroni, M. Mir, W. Knoll, *J. Phys. Chem. B.* **2007**, *111*, 13499.
[48] A. E. Kaifer, M. Gómez-Kaifer, in *Supramolecular Electrochemistry*, VCH-Wiley, Weinheim **2001**, Ch. 15, pp. 191–207.
[49] A. J. Bard, in *Integrated Chemical Systems: A Chemical Approach to Nanotechnology*, John Wiley & Sons, New York **1994**, Ch. 5, pp. 184–226.
[50] J. G. Vos, R. J. Forster, T. E. Keyes, in *Interfacial Supramolecular Assemblies*, John Wiley & Sons, New York **2003**, Ch. 3, pp. 63–70.
[51] M. Majda, in *Molecular Design of Electrode Surfaces* (Ed: R. W. Murray), John Wiley & Sons, New York **1992**, Ch. 4, pp. 159–206.
[52] R. W. Murray, *Philos. Trans. R. Soc. A: Math. Phys. Eng. Sci* **1981**, *302*, 253.
[53] R. W. Murray, in *Electroanalytical Chemistry*, Vol. *13*(Ed: A. J. Bard), Marcel Dekker, New York **1984**, pp. 191–368.
[54] C. E. D. Chidsey, R. W. Murray, *Science* **1986**, *231*, 25.
[55] J. M. Savéant, in *Elements of Molecular and Biomolecular Electrochemistry: An Electrochemical Apporach to Electron Transfer Chemistry*, Wiley-Interscience, New York **2006**, Ch. 2, p. 78.
[56] Y. Xie, F. C. Anson, *J. Electroanal. Chem.* **1995**, *384*, 145.
[57] S. Amarasinghe, T. Chen, P. Moberg, H. J. Paul, F. Tinoco, L. A. Zook, J. Leddy, *Anal. Chim. Acta* **1995**, *307*, 227.
[58] C. P. Andrieux, J. M. Dumas-Bouchiat, J. M. Savéant, *J. Electroanal. Chem.* **1982**, *131*, 1.
[59] S. E. Creager, P. T. Radford, *J. Electroanal. Chem.* **2001**, *500*, 21.
[60] B. Shoham, Y. Migron, A. Riklin, I. Willner, B. Tartakovsky, *Biosens. Bioelectron.* **1995**, *10*, 341.
[61] O. Azzaroni, M. Mir, M. Álvarez, L. Tiefenauer, W. Knoll, *Langmuir* **2008**, *24*, 2878.
[62] C. Padeste, A. Grubelnik, L. Tiefenauer, *Biosens. Bioelectron.* **2003**, *19*, 239.
[63] M. Wilchek, *Methods in Enzymology*, Vol. *184*, Academic Press, San Diego **1990**.
[64] W. Knoll, *Ann. Rev. Phys. Chem.* **1998**, *49*, 569.
[65] E. S. Forzani, M. L. Teijelo, F. Nart, E. J. Calvo, V. M. Solís, *Biomacromolecules* **2003**, *4*, 869.
[66] S. Ekgasit, G. Stengel, W. Knoll, *Anal. Chem.* **2004**, *76*, 4747.